Seasonal trends and relation to water level of reservoir-triggered seismicity in Song Tranh 2 reservoir, Vietnam

Grzegorz Lizurek [a,*], Konstantinos Leptokaropoulos [b], Jan Wiszniowski [a], Nguyen Van. Giang [c], Izabela Nowaczyńska [a], Beata Plesiewicz [a], Dinh Quoc Van [c], Anna Tymińska [a]

[a] *Institute of Geophysics, Polish Academy of Sciences (IG PAS), ul. Ks. Janusza 64, 01-452 Warszawa, Poland*
[b] *Ocean and Earth Science, University of Southampton, University Road Southampton, SO17 1BJ Southampton, UK*
[c] *Institute of Geophysics, Vietnamese Academy of Science and Technology (IGP VAST), A8 - 18 Hoang Quoc Viet Street, Cau Giay district, 100000 Hanoi, Viet Nam*

ARTICLE INFO

ABSTRACT

Reservoir-triggered seismicity (RTS) has the potential to generate disastrous seismic events of M6 and bigger. Song Tranh 2 (STR2) is an artificial water reservoir located in Central Vietnam. High seismic activity has been observed in this area since the reservoir was first filled in 2011. The relation between water level and seismic activity in the Song Tranh area is complex, and previous studies have led to the conclusion that ongoing STR2 seismic activity is an example of the delayed response type of RTS. However, the first phase of the activity observed after impoundment has been deemed a rapid response type. There were three stages of the reservoir filling periods: first, a period of initial impoundment, hereinafter referred to as pre-gap period (from 05/01/2011 to 10/06/2012), then a gap period (from 10/06/2012 to 31/08/2013) where reservoir impoundment stopped and water was drained to minimum exploitation level, and finally, a third post-gap period (from 31/08/2013 to 19/06/2017). In this work, we prove that the gap in the filling of reservoir results to a 2-fold rise of seismicity rate. The re-filling of the reservoir results to a drop of activity rate, roughly equal to the pre-gap period, accompanied by a significant increase of b-value. As a consequence, after the gap, the exceedance probability is significantly lower in comparison to pre-gap and gap periods. We also proved that the seismicity recorded between 2013 and 2016 manifested seasonal trends related to water level changes during wet and dry seasons. The response of activity and its delay with respect to water level changes suggest that the main triggering factor is pore pressure change due to the significant water level changes observed. The findings indicate that water load and related pore pressure changes considerably influence seismic activity and stress orientation in this area.

1. Introduction

Reservoir-triggered seismicity (RTS) is known since the 1930s in Algeria and the United States (Gupta, 2002), being recognized as one of the first anthropogenic seismicity phenomena. It also has the potential to generate disastrous events (Ge et al., 2009; Gupta, 1992), with magnitudes M > 6.0 much higher than the ones related to other types of anthropogenic seismicity (e.g. Davies et al., 2013; Foulger et al., 2018). Reservoir impoundment or water level changes accelerate the tectonic process, causing critically stressed faults to slip; however, a change in stress due to water level variations represents a small fraction of the ambient shear stress level acting on faults (McGarr and Simpson, 1997). The mechanism responsible for RTS involves elastic increases in shear and normal stress following reservoir filling, pore pressure increase due to diffusion, and coupled poroelastic phenomena due to compaction (Gupta, 2002; McGarr and Simpson, 1997). Different temporal seismic responses have been observed and classified: rapid response of seismicity, which starts with the filling of the reservoir; delayed response of seismicity, which appears after a few cycles of the water level; and continued or protracted seismicity, which lasts during the reservoir exploitation (Gupta, 2002; Simpson et al., 1988; Talwani, 1997). Correlations between water level changes and increased activity (Valoroso et al., 2009) or the occurrence of the largest events (Braun et al., 2018) are typical features of the RTS.

The level of natural seismic activity in the vicinity of the Song Tranh 2 reservoir (STR2) in Central Vietnam is very low. This area represents

---

the transition zone between the Indochina block and the East (South China) Sea, with right-lateral strike-slip movement and minor seismicity (Hoai et al., 2014). It has been found that in the period from 1775 to 1992, only 13 events were reported in this area and only one earthquake of M4.7 (in 1715) occurred near the actual hydropower reservoir site (Thuy et al., 2003). The reservoir volume is 740 million cubic meters and the water level varies between 140 and 175 m above sea level, whereas the length and width of the lake in maximum water level is about 15 and 9 km, respectively (IS EPOS, 2017). Seismic activity in the reservoir region, previously known as aseismic, began in 2011, soon after the filling of the reservoir in November 2010 and continued during the whole period considered for the study (Fig. 1). The seismicity of the STR2 area reached more than 200 events per month of completeness magnitude M_C 1 and above and up to 25 events per month of completeness magnitude M_C 1.9 and above. The depth of the events was between 0.2 and 21 km, but the majority of the events were located not deeper than 5 km (Fig. 1a). The largest earthquakes in the area occurred on September 3, 2012 (M4.2), October 22, 2012 (M4.6), and November 15, 2012 (M4.7).

The relation found between water level and seismic activity was complex, with no clear correlation identified either between these two trends or the occurrence of the strongest events, leading to the conclusion that a major part of the ongoing STR2 seismic activity is an example of the delayed response type of RTS (Lizurek et al., 2017; Wiszniowski et al., 2015), while the first phase of the activity observed after impoundment was deemed the rapid response type (Gahalaut et al., 2016). Despite the strike-slip tectonic regime, the focal mechanisms of the seismic events observed have mainly exemplified normal faulting on minor discontinuities (Lizurek et al., 2017). Tuan et al. (2017) have reported two strike-slip events of M1.5 and M1.9 in April 2015 with nodal planes following a similar orientation as the majority of normal faulting events recorded by Lizurek et al. (2017). The relation between the production cycle of filling the reservoir is investigated in this study. First, the gap in the reservoir filling, then the seasonal relation of seismic hazard parameters during filling the reservoir in the wet season and releasing the water during the dry season in the post-gap period are the main subjects of the present work. We also examine how average seismic activity is related to the changes in water level and whether it implies variation of the principal stress during seasonal fluctuations of water levels in the reservoir.

2. Methods

The monitoring campaign comprised three stages with different
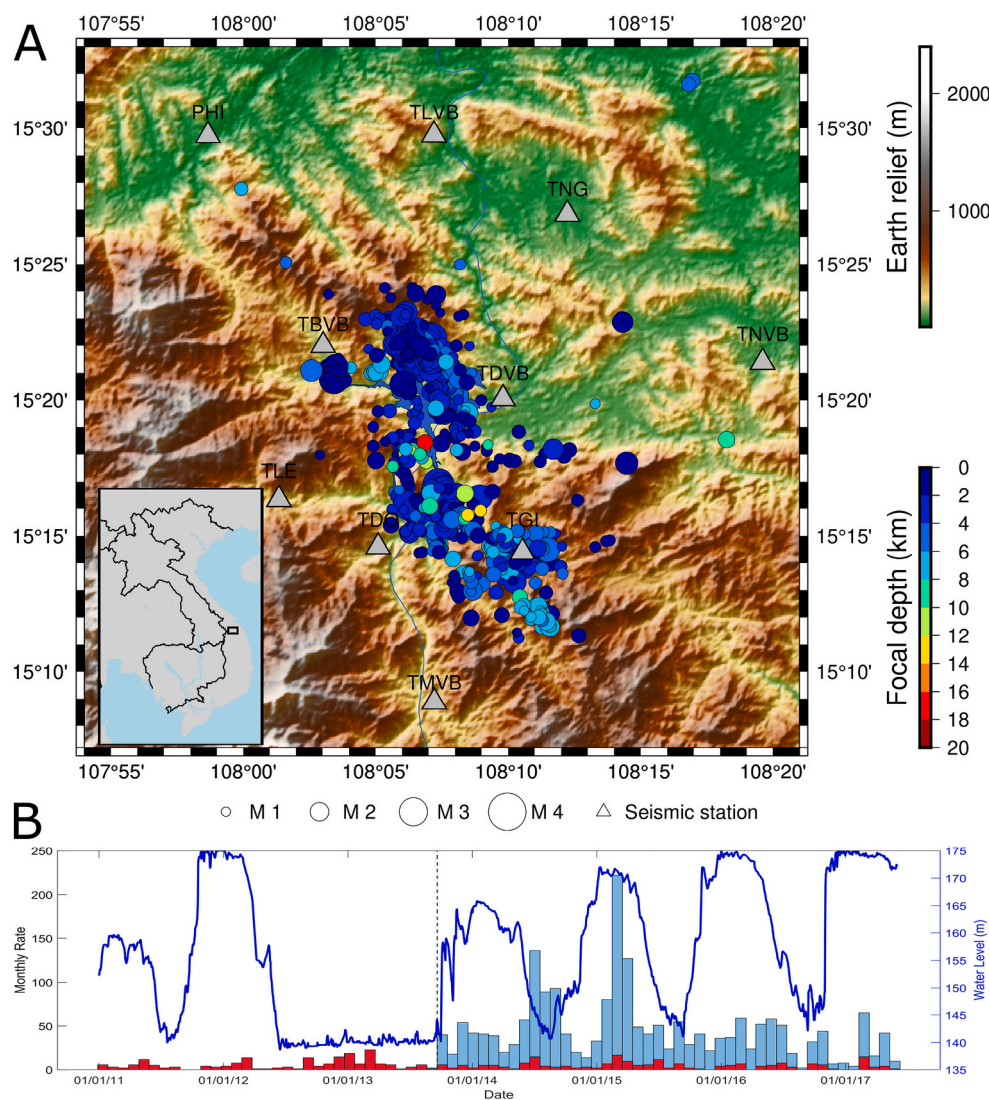
Fig. 1. Location and activity rates of seismicity in Song Tranh area after reservoir impoundment: (a) Location of seismic events with M ≥ 1, (b) Water level and monthly activity rate for events of M ≥ 1 (blue bars) and events of M ≥ 1.9 (red bars). (For interpretation of the references to colour in this figure legend, the reader is referred to the web version of this article.)

numbers of stations, including 10 local stations deployed in the vicinity of STR2 (Fig. 1). These stages correspond to the reservoir filling periods: first, a period of initial impoundment, hereinafter referred to as pre-gap period (from 05/01/2011 to 10/06/2012), then a gap period (from 10/06/2012 to 31/08/2013) where reservoir impoundment stopped and water was drained to minimum exploitation level, and finally, a third post-gap period (from 31/08/2013 to 19/06/2017). The spatial distribution of events and stations in every phase is shown in Fig. 2. Before and just after the beginning of filling the STR2 reservoir, the area was monitored by two seismic stations in Binh Dinh and Hue, being located away from the reservoir (located outside the area zoomed in Fig. 1 and Fig. 2). The more precise monitoring of the triggered seismicity in the STR2 reservoir was installed from October to November 2012, when a five stations network was deployed by Institute of Geophysics Vietnamese Academy of Science and Technology (IGP VAST) in the STR2 reservoir and vicinity. They were equipped with Guralp 30s

seismometers and the SAMTAC logger and one Trillium-40 seismometer with the Q330 logger. The third stage of the monitoring started in August 2013, when 10 seismic stations were installed. This seismic network was called VERIS (Vietnam Reservoir Induced Seismicity). Stations provided by Institute of Geophysics Polish Academy of Sciences were equipped with short-period seismometers Lennartz LE-3DLite (1 s), and those provided by IGP VAST were equipped with long-period seismometers Guralp CMG-6TD (30s). Signals from seismometers Lennartz were recorded with a sampling rate of 100 samples per second (sps) and dynamics 132 dB. Seismometer Guralp has an on-board digitizer with a dynamic of 130 dB and a sampling rate of 100 sps. Both systems are appropriate to measure local and regional seismicity, as the main content of seismic waves comes in the range of a few Hz, whereas Guralp stations were more suitable for the largest events in the STR2 region due to the lower frequency dominating in such recordings. The location of the hypocentres was determined with the use of the LocSAT application
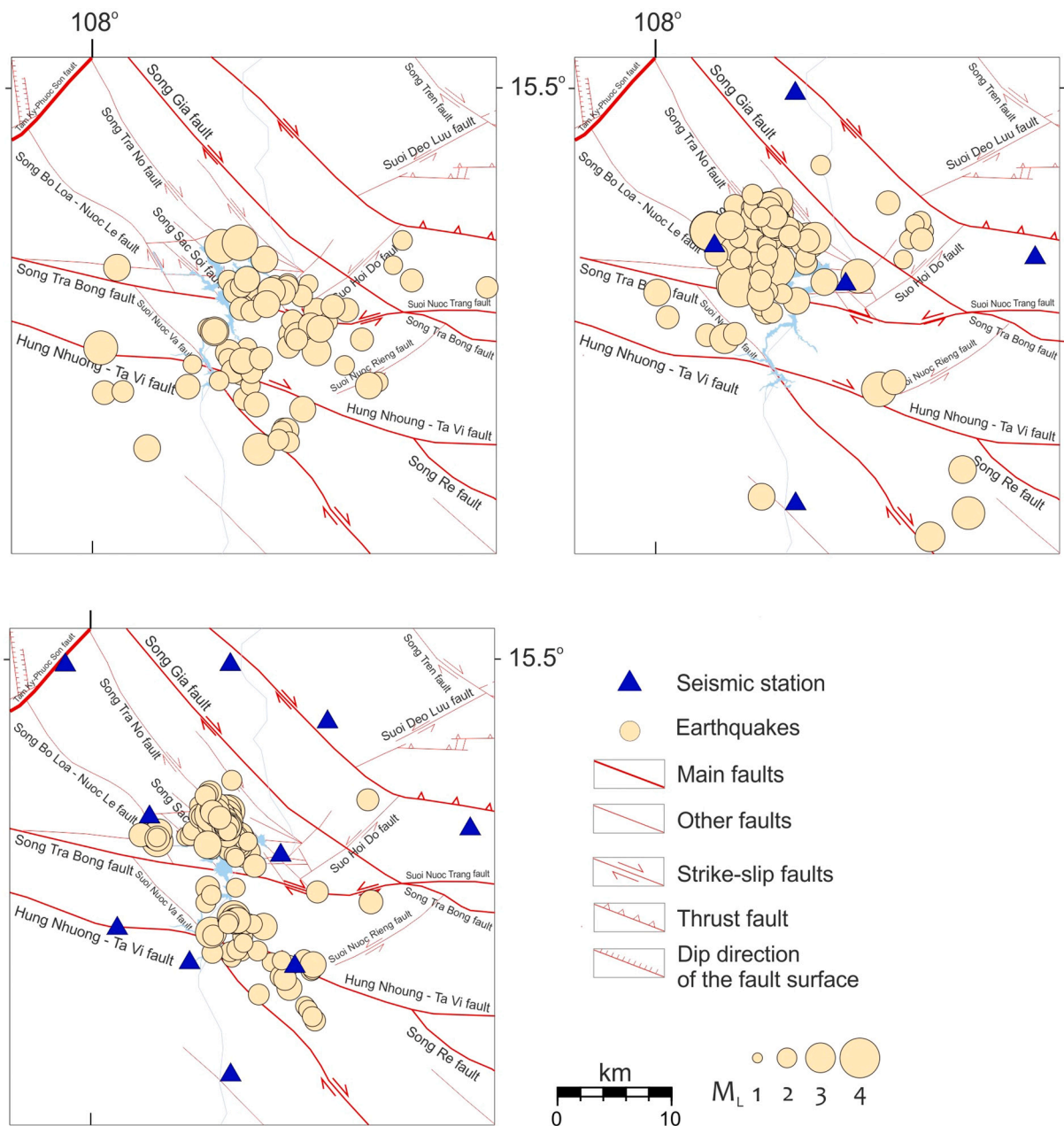

Fig. 2. Spatial distribution of stations and events locations clockwise from upper left: pre-gap period (from 05/01/2011 to 10/06/2012), gap period (from 10/06/2012 to 31/08/2013), and post-gap period (from 31/08/2013 to 19/06/2017), respectively.

based on ray-tracing approach and 1D velocity model (Bratt and Bache, 1988) within routine manual picking. Epicentral location errors varied from 0.5 to 9 km depending on the number of stations and magnitude of the events. Most of the location errors for the events above Mc = 1 were in the range between 0.5 and 2 km. P- and S-wave time residuals of picking were within the range between −0.3 and 0.3 s for the majority of events. Depth location error was mainly not bigger than 1 km. However, when the estimated depth was unrealistic its value was fixed at 5 km. We used local magnitude (M_L) calculations based on Richter's (1936) formula with the original Richter's (1958) distance correction term to keep the consistency of magnitude estimates within different stages of the monitoring. The spatial distribution of stations and events is shown in Fig. 1. Details of the equipment in all monitoring phases can be found in Wiszniowski et al., (2015). Data about the seismic network, basic catalog of seismic events as well as waveforms for the third stage of the monitoring are available on the EPISODES Platform website dedicated to Song Tranh triggered seismicity (IS EPOS, 2017).

Seasonal patterns of seismicity were based on monthly activity variations. This analysis aimed to quantify how "seasonal" patterns remain uniform over time and to either accept or reject the uniform pattern hypothesis under a given confidence level. This would allow us to capture temporal pattern in anthropogenic trends associated with water reservoir exploitation. The main part of this analysis was to test whether the observed time patterns were significantly different against the ones derived from reshuffled series. The reshuffled series were configured accordingly, to ensure an equal number of events, in the same range of value (e.g. Lemarchand and Grasso, 2007; Tahir et al., 2012), allowing us to accept or reject the observed seasonal trend at a given (e.g., 95%) confidence level. We performed Monte Carlo simulations (e.g., Grasso et al., 2018; Lemarchand and Grasso, 2007; Tahir et al., 2012), involving 1000 random sets of key events. The 1000 synthetic sets were then analyzed in the same manner as the real seismicity catalog to assess the confidence levels for the observed episode distribution. Seasonal and monthly variations in seismicity were also compared with the water and precipitation levels in the study area.

To account for the influence of water level in seismic activity, instead of focusing only on seismicity rate changes, we adopt a novel approach, incorporating both activity rate and magnitude distribution of the seismic events. This approach does not only offer a more complete characterization of seismicity but also can be used as a measure of seismic hazard variation through time, in connection to the water level fluctuations. For this purpose, the Mean Return Period (MRP) and the Exceedance Probability (EP) are calculated using the SHAPE software package (Leptokaropoulos and Lasocki, 2020).

Considering the earthquakes with magnitudes greater than or equal to the completeness magnitude ($M \geq Mc$), the MRP is defined as the average time elapsed between two successive events with magnitude $M \geq M_t$ as:

$$MRP = \left[\lambda \left(1 - F_M(M_t) \right) \right]^{-1} \tag{1}$$

where, λ, is the mean seismic activity rate, M_t is referred to as target magnitude, and F_M is the cumulative distribution function (CDF) of the magnitudes. The EP of an event with magnitude greater than or equal to M_t, within a specified target time period, T_t, is defined as:

$$EP = 1 - e^{-\lambda T_t \left(1 - F_M \right)} \tag{2}$$

F_M can be determined by either parametric (e.g. Gutenberg-Richter law) or by non-parametric (data driven) approaches. In this study, the dataset, as well as subsets corresponding to different time periods, were tested as a function of magnitude cut-off (M_{cut}) by means of the Anderson-Darling test (Leptokaropoulos, 2020), in order to verify the validity of the Gutenberg-Richter law. In all cases tested it was found that the hypothesis of exponential magnitude distribution could not be rejected at 0.05 significance level for cutoff level $M_{cut} \geq 1.0$ (for the seismicity between 2013 and 2017) and $M_{cut} \geq 1.9$ (for the seismicity

between 2011 and 2013). This means that the Gutenberg-Richter law provides a sufficient approximation of the magnitude distribution, considering $M_C = 1.0$ and $M_C = 1.9$, respectively. Therefore, when we study the entire time period (2011-2017) we apply the highest value $M_C = 1.9$. Furthermore, based on the historical records, the limited dimensions of the study area and the local tectonic structures (Lizurek et al., 2017) the upper-bounded Gutenberg-Richter law (Page, 1968) was selected as the appropriate model with CDF:

$$F_M(M) = \begin{cases} 0 \; for \; M < M_C \\ \dfrac{1 - e^{-\beta\left(M - M_C + \frac{\Delta M}{2}\right)}}{1 - e^{-\beta\left(M_{max} - M_C + \frac{\Delta M}{2}\right)}} \; for \; M_C \leq M \leq M_{max} \;, \\ 1 \; for \; M > M_{max} \end{cases} \tag{3}$$

where ΔM is the magnitude reporting accuracy (0.1 is this study) and β is connected to the well-known b-value as $\beta = b \cdot \ln(10)$. The maximum likelihood estimation of β is calculated as the root of the equation:

$$\frac{1}{\beta} + \frac{\widehat{M}_{max} - M_C + \frac{\Delta M}{2}}{1 - e^{\beta\left(\widehat{M}_{max} - M_C + \frac{\Delta M}{2}\right)}} - \langle M \rangle - M_C + \frac{\Delta M}{2} = 0 \tag{4}$$

M_{max} is the upper bound of magnitude distribution, estimated by the usage of the generic Kijko and Sellevoll (1989) formula:

$$\widehat{M}_{max} = M_{cat} + \int_{M_c}^{M_{cat}} [F_M(M)]^n dM, \tag{5}$$

where M_{cat} is the largest observed magnitude value in the n-element complete catalog. Eq. (5) provides a biased estimation of M_{max}, therefore its result is further corrected according to Lasocki and Urban (2011). After the correction applies and given all the available regional data (2011-2017), the maximum magnitude in the study area was found equal to $M_{max} = 5.0$. The confidence interval of hazard parameters (MRP and EP) and b-values were estimated by a bootstrap resampling approach based on the work of Orlecka-Sikora (2008).

Target magnitude, M_t for MRP and EP was set equal to 3.5 and target time period (T_t) for EP was set equal to 30 days. Although arbitrarily selected, the choice of the aforementioned values does not aim at obtaining exact hazard values for engineering purposes, but rather at comparing how these hazard parameters (MRP and EP) vary in time and whether their variation is significant within subsequent time windows. Since absolute result values are not important for the purposes of this analysis (retrospective comparative study), any set of parameters would provide identical results.

Seasonal variations in stress orientation during wet and dry periods were analyzed, too. The main stress directions of the study area were derived from focal mechanisms. All data processing: location, picking were performed manually after visual inspection of waveform quality. Initially, moment tensors (MT) were obtained by inversion of the P-wave amplitudes in the time domain (Kwiatek et al., 2016; Wiejacz, 1992). Due to the sparse network and insufficient data, 90 MT solutions were available (Lizurek et al., 2017). One of the possibilities to increase the number of focal mechanism estimations was to include the S-wave amplitudes into the procedure of the MT inversion. According to Aki and Richards (2002), Fitch et al. (1980), and De Natale et al. (1987), the recorded displacement for the P- or S-wave phase is:

$$\mathbf{U}^P(\mathbf{x}, t) = \frac{\boldsymbol{\gamma} \cdot \dot{\mathbf{M}}\left(t - T^P\right) \cdot \boldsymbol{\gamma}}{4\pi\rho\alpha^3 r} \mathbf{I}$$

$$\mathbf{U}^{SV}(\mathbf{x}, t) = \frac{\widehat{\mathbf{P}}_\gamma \cdot \dot{\mathbf{M}}\left(t - T^S\right) \cdot \boldsymbol{\gamma}}{4\pi\rho\beta^3 r} \widehat{\mathbf{P}}_\mathbf{I} \tag{6}$$

where ρ is the average medium density, r is the source-receiver distance, α and β are the average velocities of the P- and S-waves at the source, T^P and T^S are the travel times of the P- and S-waves, **M** is the seismic MT, **l** is the wave direction at the receiver, γ is the wave direction at the source, and $\hat{\mathbf{P}}_\gamma$ and $\hat{\mathbf{P}}_l$ are transverse directions at the source and the receiver.

A MT is obtained by solving a set of N equations of type (6), where N is the number of seismic phases at stations recording the event. Uncertainties of the estimated MT can be estimated through the normalized root-mean-square (RMS) error between theoretical and estimated amplitudes (Stierle et al., 2014a, 2014b):

$$RMS = \sqrt{\frac{\sum\limits_{i=1}^{N}\left(U_i^{measured} - U_i^{th}\right)^2}{\sum\limits_{i}^{N}\left(U_i^{measured}\right)^2}} \qquad (7)$$

The validation of the extended method was prepared first comparing solutions obtained by the use of synthetic amplitudes of assumed faulting for different network setups, with all the results properly resolved. Similar tests were described by Lizurek (2017) and Lizurek et al. (2019) for another reservoir in Vietnam. For VERIS network synthetic tests for MT P- and S-wave amplitude inversion was performed for normal and reverse fault with assumed geometry 304/71/±108 (strike/dip/rake) with double-couple (DC) component changing in the range 0% to 100%. Tests were performed for six depths: 500 m, 800 m, 1 km, 2 km, 3 km, 5 km, and 8 km. Moreover, synthetic Gaussian noise was added in amounts up to 10%, 20%, 30%, 40%, and 60% of the amplitude. All solutions have low RMS error, which mainly exceeds 0.3 only for the highest tested noise level, while for the other noise levels it is mostly below 0.3 (Fig. 3). MT solutions were stable for unbiased data for assumed mechanisms with more than 50% DC, however the proportion of calculated components was in accordance with the assumed ones (Table 1). Jackknife single station rejection test for both normal and reverse geometry showed that there is no crucial station, which influences the result stability. Solutions remain stable regardless of the station rejection if the solution for all stations was reliable. For noise contamination, the reverse mechanism occurred more reliable with lower RMS error and with stable solutions for all examined depths if the
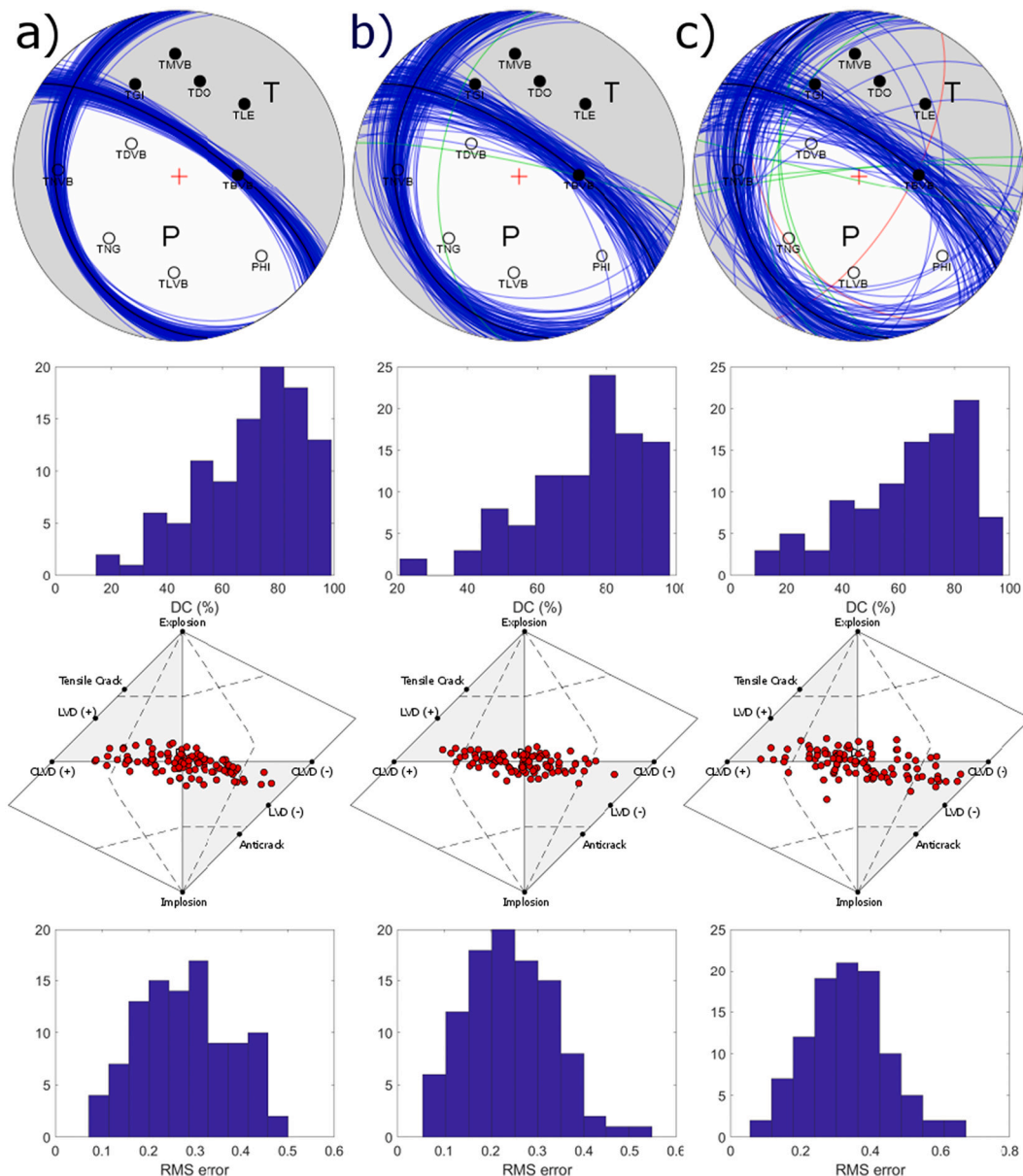

Fig. 3. Full MT solutions obtained in resampling bootstrap test for VERIS: a) up to 20%, b) up to 40% and c) up to 60% noise contamination.

Table 1
Moment tensor solutions (full, trace null, and double couple) for events with different assumed mechanisms resolved for VERIS network.

Assumed mechanism	VERIS- normal fault			VERIS- reversed fault		
	Full solution	Deviatoric solution	DC solution	Full solution	Deviatoric solution	DC solution
10 % DC						
20 % DC						
30 % DC						
40 % DC						
50 % DC						
60 % DC						
70 % DC						
80 % DC						
90 % DC						
100 % DC						

mechanism has more than 50% DC. For normal fault mechanisms events with the high non-DC component for depths lower than 3 km should be considered carefully. Limitations of MT inversion for VERIS network seem to be mainly connected with non-DC types of events, which are unlikely to occur in reservoir triggered seismicity on existing tectonic discontinuities. The second step of the validation was based on a comparison between the already existing solutions obtained with P-wave amplitudes. We calculated the Kagan angle (Kagan, 1991) between new and solely P-wave MT solutions. The solutions with a high Kagan angle indicated low-quality solutions (this was additionally checked with the RMS of the solutions). In such cases, the lower RMS solution (RMS < 0.3) was taken into account and if the RMS was greater than 0.3 both solutions were rejected. Subsequently, all the events with a reasonable signal to noise and P- and S-wave amplitudes were processed. This resulted in MT solutions for 180 events from August 28, 2013 to October 19, 2016 (Fig. 4).

Stress inversion was based on all 180 events with associated MT solutions (Fig. 5). The stress inversion was estimated using the Michael (1984) method modified by Vavryčuk (2014). The inversion provided the orientations of the three principal stress axes and a shape ratio R (Gephart and Forsyth, 1984), expressed as follows:

$$R = \frac{\sigma_1 - \sigma_2}{\sigma_1 - \sigma_3} \tag{8}$$

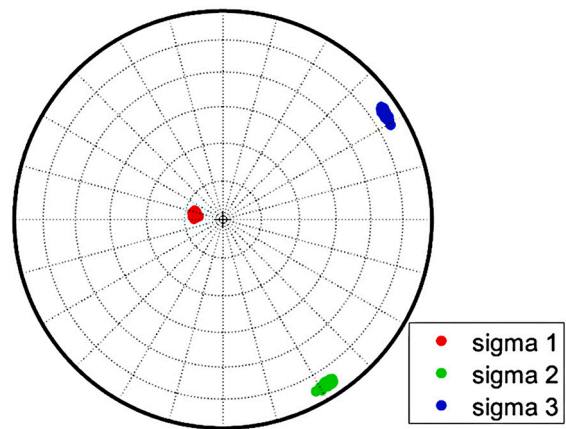where σ_1 to σ_3 are the magnitudes of the three principal stress axes.

Fig. 5. Principal stress orientation in the STR 2 area derived from 182 focal mechanisms. Areas of 90% confidence intervals from bootstrap tests denoted in red, green, and blue for σ_1, σ_2, and σ_3, respectively. (For interpretation of the references to colour in this figure legend, the reader is referred to the web version of this article.)

3. Results

The seismicity of the STR2 area during the study period is relatively high, varying from several tens to more than 200 events per month of magnitude M_C1 and above (Fig. 1). The vast majority of the events are located at <25 km from the center of the lake. The analysis is therefore
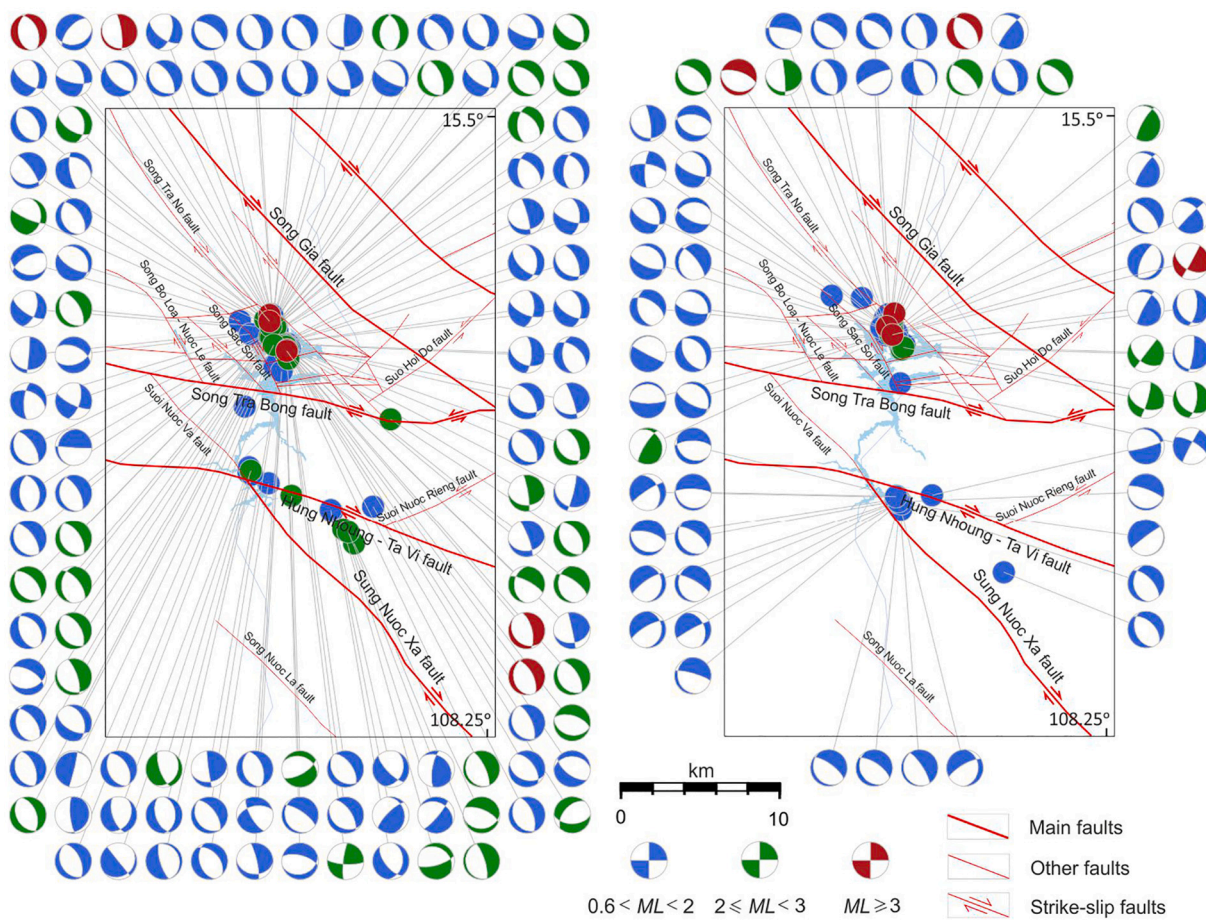

Fig. 4. Spatial distribution and focal mechanism examples obtained for the available data: dry season: January–July (left) and wet season: August–December (right). The magnified area is denoted with a red rectangle in Fig. 1. (For interpretation of the references to colour in this figure legend, the reader is referred to the web version of this article.)

restricted in an area centered approximately to the center of the lake within a radius of ~25 km, where 99.5% of the recorded events are located. The biggest recorded event in the post-gap period was a $M_L 3.6$ and occurred on September 17, 2014. The depths of the events were shallow, usually no deeper than 8 km. Focal mechanisms were obtained for events located in the above defined area. MT solutions with an RMS of a full MT solution of up to 0.3 were obtained for 180 events of $0.7 \leq M_L \leq 3.6$ recorded between August 28, 2013 and October 19, 2016. The observed seismicity mostly exemplified normal faulting with a NW-SE strike (Fig. 4), with almost vertical principal stress σ_1 and horizontal σ_3 striking to NE (Fig. 5).

Table 2 shows the properties of seismicity before and after September 2013, when the reservoir impoundment continued after an almost 1-year gap. The completeness magnitude was estimated equal to 1.9 for the 2011–2013 period. This cut-off value was adopted for the entire dataset (2011-2017) in order to achieve a proper comparison of seismicity properties. As shown in Table 2, higher seismicity rates and maximum magnitudes are observed before September 2013. Most important, b-values are significantly lower before and during the gap, in comparison to the post-gap period (statistically significant difference at 95% level).

Hazard parameters for the three datasets corresponding to pre-gap, gap, and post-gap periods, respectively, were calculated for $M_{cut} = 1.9$ (Fig. 6). It is demonstrated that the gap increases the exceedance probability (equivalently, decreases the mean return period) of $M \geq 3.5$ events. The rate of $M \geq 1.9$ events doubles during the gap and returns roughly to the pre-gap level in the post-gap period. On the other hand, the b-value does not change during the gap, however, it rises significantly after the gap, resulting together with the decreased seismicity rate in a substantial exceedance probability drop. The gap doesn't influence the b-value, but it results in a 2-fold rise of seismicity rate. The re-filling of the reservoir results in a drop of activity rate, roughly equal to the pre-gap period, accompanied by a significant increase of b-value. As a consequence, the exceedance probability is significantly lower after the gap in comparison to pre-gap and gap periods.

Seasonal trends were calculated for a complete catalog covering the post-gap period from August 2013 to January 2017. The improved network performance resulted in a magnitude of completeness equal to 1.0 estimated using a catalog-based goodness-of-fit (GFT) test method at 95% confidence bounds (Wiemer and Wyss, 2000). The results of the monthly seasonal trends of seismic activity based on stacked monthly activity rates in the STR2 area are presented in Fig. 7. Activity exceeding the mean background pattern is observed in February, March, and July. Significantly lower activity than the mean activity pattern is observed during August, November, and December. This pattern in form of the average monthly activity rates was then compared with the average precipitation and water levels during the study period (Fig. 8). It is shown that water is mainly gathered during the period from September to December, when the average rainfall is the highest. During this period, the level of activity is low, in September and October being close to average, and then decreasing significantly below the average. By contrast, the average water level rises from the average minimum in August until December, when it reaches its highest value, and then remains stable until April when it is discharged until August, reaching the average minimum water level. The highest mean seismic activity is

reached in February–March and in July. The first two-month period of increased activity is longer and is delayed by about two months to the time when the reservoir's optimum storage capacity is reached. The second increased activity period is observed during the water discharge period, about two months after the water level starts to decrease during the dry season. This trend is similar to that observed in 2012, when the biggest events took place after draining the reservoir to the minimum level (Wiszniowski et al., 2015 and Fig. 5). The seismic activity increase is delayed by about two months to the maximum water level and the beginning of the water discharge. The temporal variation of hazard parameters was investigated in connection to reservoir water level, after the gap (from June 2013 and after). Various trials were performed for different time windows created as either equal time duration (ΔT) or equal event number (NT) datasets. The Spearman Correlation Coefficient (SCC) was considered as a measure to quantify the correlation between water level and hazard parameters. SCC is a non-parametric estimator measuring the dependence of the ranking of two random variables, defined as:

$$SCC = 1 - \frac{6 \sum r_i^2}{n(n^2 - 1)} \qquad (9)$$

where r_i is the difference between the two ranks of each variable and n is the number of observation points (variables pairs). The closest to 1, the stronger the linear correlation between the 2 variables. We also estimate the *p*-value, which quantifies the significance of the hypothesis that no correlation between the two variables exists. A p-value below 0.05 is routinely assumed to be a strong indication of a linear correlation. Attempts with non-overlapping time windows with $\Delta T = 30, 50, 100$ days and event windows with NT = 50 and 100 events, didn't result in any significant correlation between either b-value/ EP/ MRP and water level (SCC was always ~0.0). Cross-correlation analysis indicated, however, that the maximum correlation is achieved at zero time lag (note that 'zero time lag' does not indicate a specific time interval because the window size differs in each trial).

Since no short term correlation could be established, we further sought for potential seasonal phenomena. Seasonality effect was determined based on the information of the climate in central Vietnam (IPONRE, 2009), exhibiting 2 distinct seasons: A "Dry" season (7 months: January to July) and a "Wet" season (5 months: August to December), which is in agreement with the seasonal precipitation trends observed in the studied area (Fig. 8). Note the uneven duration of the two seasons (5 months wet season, 7 months dry season). The correlation between hazard parameters and the water level was then estimated for the subsequent cycles, each one comprises the two aforementioned seasons. Fig. 9 shows that the EPs are, in general, higher during the dry season (Note that as far as MRP is concerned, in all cases, SCC has the same value and opposite sign as EP). The seismicity rate also seems to follow a correlated pattern, since each dry season always demonstrates a higher seismicity rate in comparison with the prior and posterior wet seasons. However, no clear pattern can be extracted for the b-values. Correlation analysis considering the 4 cycles (8 seasons) indicates that the SCC between EP and water level is 0.55 ($p = 0.171$) and between b-value and water level is 0.48 ($p = 0.243$). SCC is quite high, indicating some level of correlation, however this result is not significant at 0.05 confidence level. If we discard as an outlier the anomalous results of the

Table 2

Seismicity properties before and after the impoundment gap, lasted till 1st of September 2013, when the reservoir started to refill. The second column indicates the magnitude cut-off value. The third column shows the number of events above M_{cut}. The fourth and fifth columns depict the estimated b-value and its corresponding 95% confidence interval, respectively. The sixth column represents the seismic activity rate, whereas the seventh column shows the duration of each study period. The maximum observed magnitude recorded in each period is shown in the last column.

Period	M_{cut}	$N_{(M \geq Mcut)}$	b	$bCI_{95\%}$	Rate (events/day)	Duration (days)	M_{maxobs}
Before 09/2013	1.9	189	0.79	0.684–0.896	0.20	945	4.7
After 09/2013	1.9	213	1.14	0.996–1.304	0.155	1378	3.6
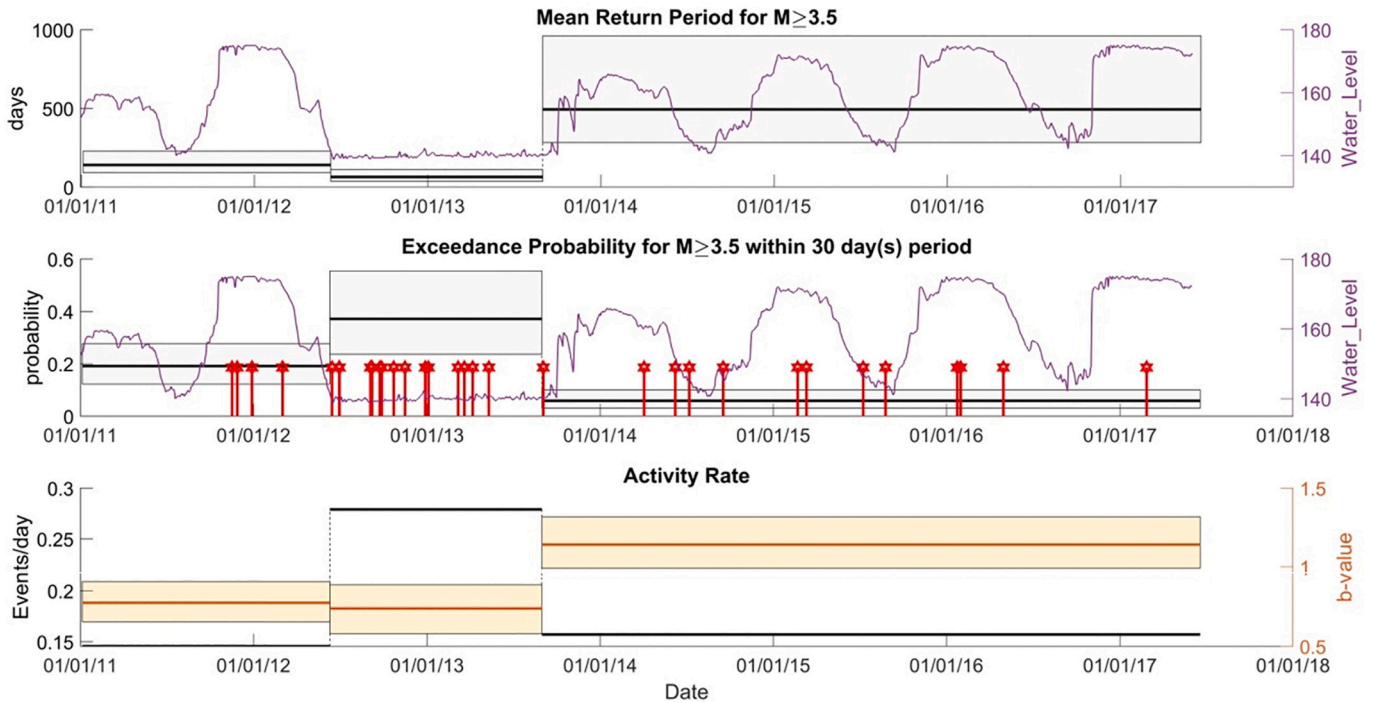
Fig. 6. Upper frame: Mean return period (horizontal lines) and water level (purple curve) for the three study periods (from left to right; pre-gap, gap, and post-gap periods). Middle frame: Exceedance probability (horizontal lines) and water level (purple curve). Lower frame: Mean activity rate (black lines) and b-values (orange lines). The shaded areas indicate the 95% confidence interval of the corresponding parameters. Stems indicate the occurrence of $M \geq 3.0$ events. (For interpretation of the references to colour in this figure legend, the reader is referred to the web version of this article.)
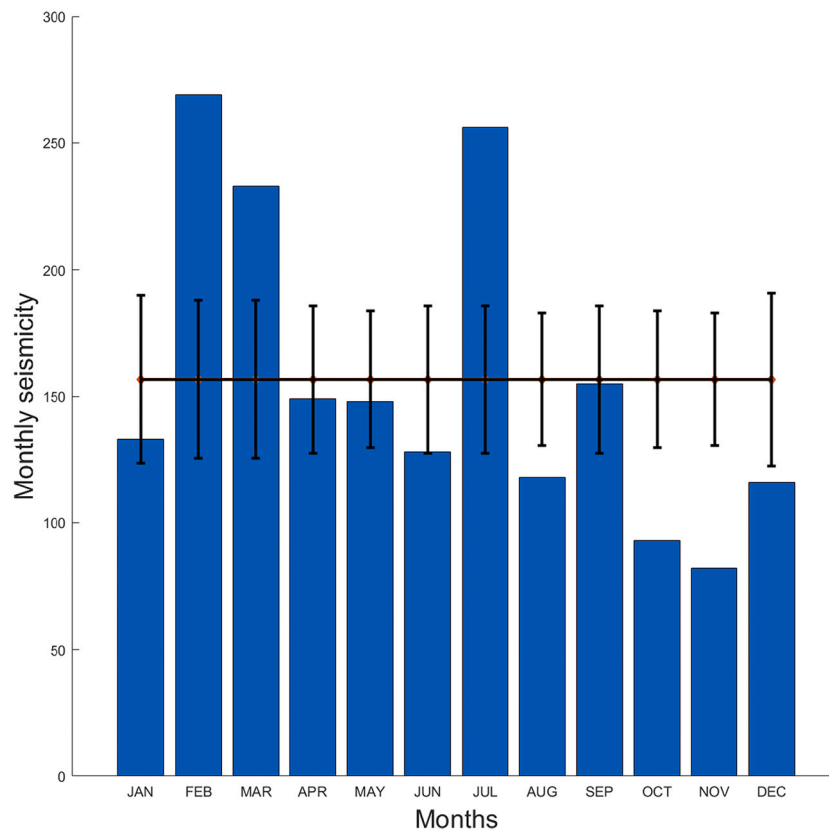
Fig. 7. Seasonal trends in seismicity of STR2 during 3 full years of post-gap period (September 2013–August 2016). Monthly stacked seismic activity (bars) with randomized mean activity estimate (solid line) and its variability range (error bars).
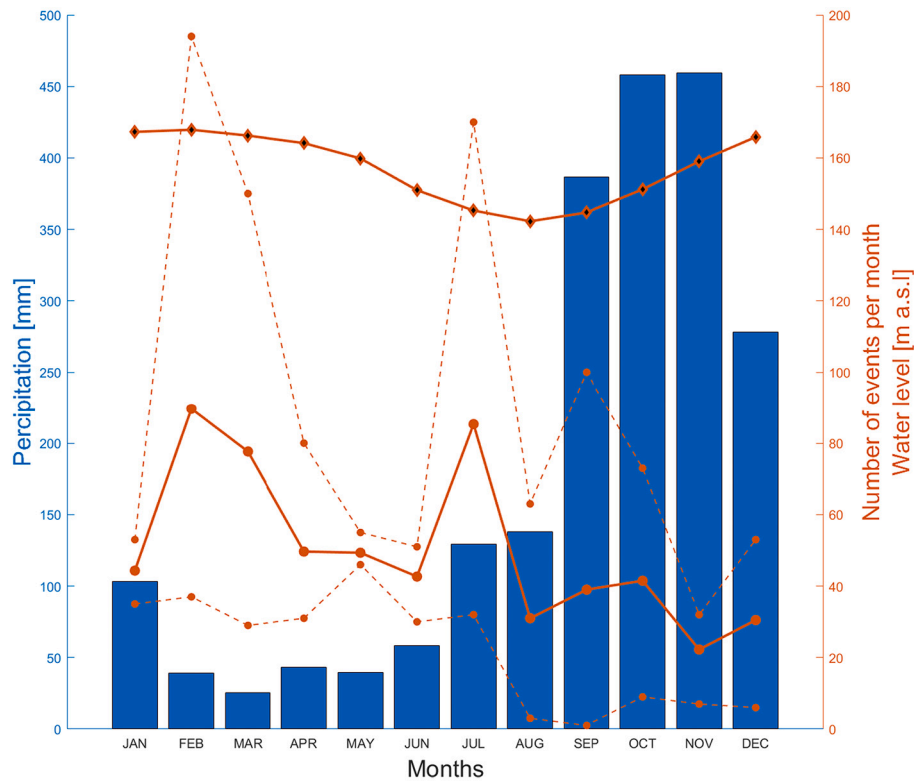
Fig. 8. Monthly average precipitation derived from Da Nang and Hue meteorological stations (bars), monthly average water level (solid line with diamonds), monthly average seismic activity (solid line with dots) maximum and minimum monthly activity (dashed line with dots) in the STR2 area.
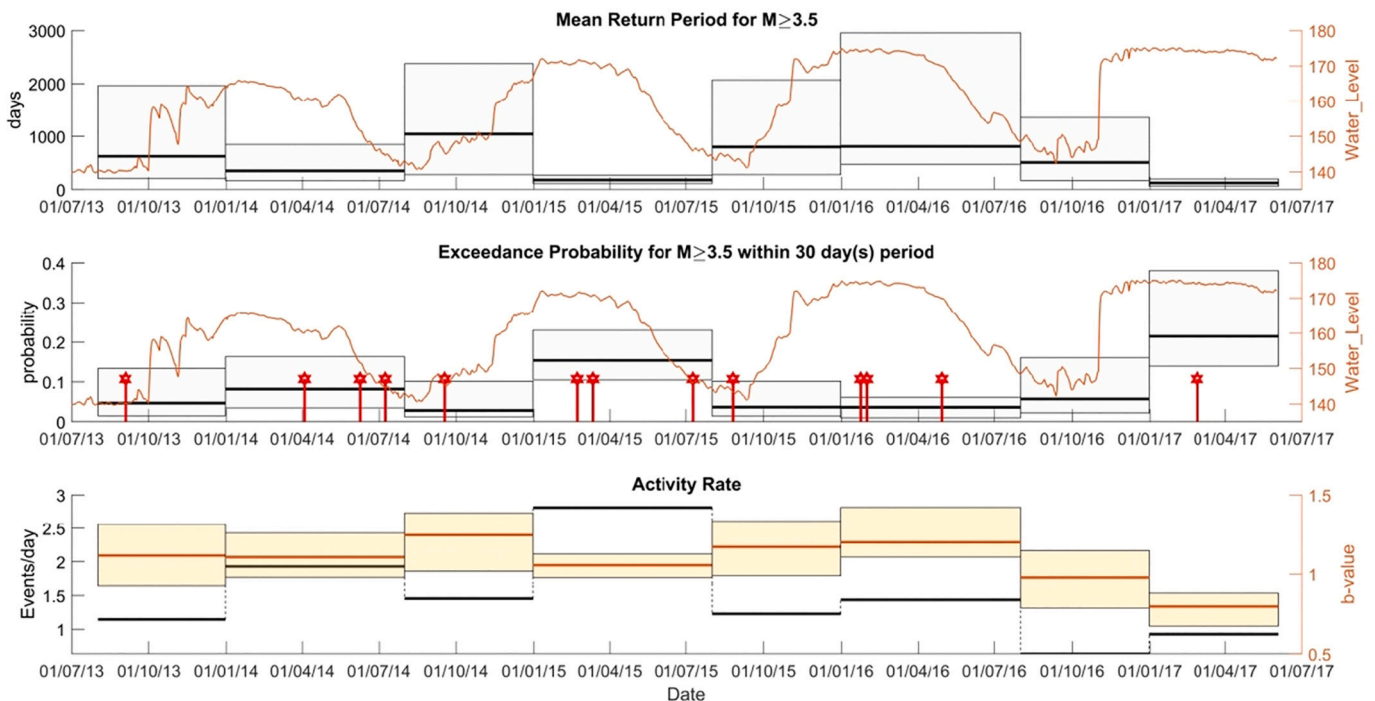

Fig. 9. Hazard parameters for subsequent seasons (wet-dry), considering the GRT magnitude distribution model. The parameters were set as: $M_C = 1.0$, Tt = 30 days, Mt. = 3.5, $M_{max} = 5.0$, Notation as in Fig. 4.

sixth period, the corresponding SCC between EP and water level is 0.89 ($p = 0.012$) and between b-value and water level is 0.78 ($p = 0.048$). The result in this case, although statistically significant, cannot be decisive due to the limited number of observations (7 samples) and the omission of one period. Thus, in order to strengthen the significance of the seasonal effect by eliminating the small sample influence, the seismicity data were aggregated into two groups, one corresponding to winter seasons and one to the summer seasons, respectively. In such a way a

Table 3

Seismicity rate, b-value, and hazard parameters corresponding to four aggregated dry seasons (2nd column) and four aggregated wet seasons (3rd column). Values in the brackets indicate the 95% bootstrap CI. EPs and MRPs are significantly different at 95% level.

Parameter	Dry Season (1st January to 31st July)	Wet Season (1st August to 31st December)
Rate *(events/ day)*	1.70	1.05
b-value	1.063 [1.013–1.121]	1.148 [1.061–1.225]
EP (GRT)	0.092 [0.067–0.121]	0.036 [0.023–0.059]
MRP (GRT) *days*	310 [232–434]	820 [495–1280]

clear seasonal correlation pattern is revealed (Table 3). It is shown in Table 3 that seismicity occurred during dry seasons demonstrates higher rates and lower b-values than during wet seasons, although the b-values difference is not statistically significant. On the other hand, the 95% confidence intervals of EP as well as of MRP do not overlap with each other, indicating a significant difference of these hazard parameters between dry and wet seasons. The EP of an $M = 3.5$ event within a 30-days period is 2.5 times higher within the dry season than it is during the wet season. It is worth mentioning that during the first three cycles there is one event with $M \geq 3.0$ per wet season (low EP) and three events with $M \geq 3.0$ per dry season (high EP) (Fig. 9).

Small differences can be identified in stress orientation during dry (118 events with MT) and wet seasons (62 events with MT, Fig. 10). A stress inversion was calculated for the MT solutions obtained in these periods. Principal stress σ_1 during the dry period is almost vertical with $12°$ trend and its azimuth to WWN, while σ_1 during the wet period trends more to the west and is more vertical trending to $8°$. The σ_1 orientation 90% CI slightly overlaps. The same applies for σ_2, while the CI of the σ_3 orientations overlap significantly (Fig. 10). It is also clearly visible that the scatter of the principal stress orientation obtained for the wet period is bigger when compared with the stress inversion results of the dry period. The latter is a result of the difference in the number of events available for inversion in the considered periods.

4. Discussion

The major part of seismicity in the STR2 area (post-gap period) represents an example of delayed response RTS. Nevertheless, the first phase of the activity observed after impoundment was deemed the rapid response type (Gahalaut et al., 2016). There is no direct relation
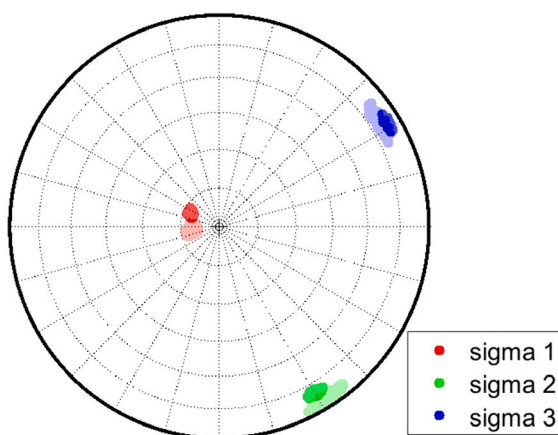
Fig. 10. Principal stress orientation in the STR2 area in dry (solid colors) and wet (transparent colors) seasons. Areas of 90% confidence intervals from the bootstrap tests denoted with red, green and blue for σ_1, σ_2, and σ_3, respectively. (For interpretation of the references to colour in this figure legend, the reader is referred to the web version of this article.)

between the occurrence of the highest magnitude event or activity increase and water level (Lizurek et al., 2017), but according to our findings, activity changes are related to changes in water level; both the gap in the reservoir filling and the seasonal cycle have significant influence on seismic activity and $M \geq 3.5$ events occurrence probability (Fig. 6 and Fig. 9). The exceedance probability of $M \geq 3.5$ events increases during the gap, when the water reservoir is kept at its minimum capacity due to maintenance reasons. The rate of $M \geq 1.9$ events doubles during the gap and returns roughly to the pre-gap level in the post-gap period. After the gap, the exceedance probability is significantly lower in comparison to pre-gap and gap periods. This suggests that the filling cycle stabilizes the activity and stress release, while the almost one-year gap in filling results in a substantial water load and pore pressure decrease, which triggers the $M \geq 3$ events more frequently than during the normal water-filling cycle. Taking into account that the main stress orientation derived from the focal mechanism is a normal faulting type with an almost vertical pressure axis and NW-SE dominant strike of nodal planes, it seems that the decrease of water load and subsequent pore pressure change are decreasing the horizontal stresses more than the dominant vertical one. This is followed by a decrease of normal stress which makes faults in the STR2 more prone to rupture. It is worth noting that main discontinuities and seismic events are located within 20–25 km radius from the lake and mainly between 2 and 8 km below the surface. Change in pore pressure due to the water level decrease is extensional in all directions, thus reduces the compressive normal stresses at any point and promotes shear failure. This means that the stress change from the reservoir is diffused rather horizontally toward the active discontinuities, and the maximum vertical stress is affected less than the horizontal ones. Normal faulting is triggered by vertical stress caused by the mass of water and pore pressure, the other types should be expected as results of coupled poroelastic effects and/or diffusion (Scholz, 2019). The above statement is applicable to the increase of vertical stress due to water level increase, while in our case we observe higher seismicity rates when the water level is decreased and the vertical stress is decreased less than the horizontal ones. This causes a relative increase of vertical stress in comparison to horizontal ones resulting in normal faulting triggering. This should be confirmed with detailed pore-pressure, and Coulomb Stress modeling, which is beyond the scope of this work, but seems to be a reasonable next step in Song Tranh seismicity studies.

We can distinguish two water level periods in the annual reservoir exploitation cycle. First, from January to July, when there is a high water level up to May, when water is stored in the reservoir. The second period starts in August, when the annual minimum of the water level is reached (Fig. 8). The main activity bursts are observed during low and high water level periods from 31/08/2013 to 19/06/2017 (post-gap period), but mainly in the winter season (February, March, and July; Fig. 8), suggesting a delayed response to the water level changes, which are followed by pore pressure and stress changes in the vicinity of the reservoir. The highest average and maximum activity observed in post-gap period for February, March, and July, the same applies to the difference between maximum and minimum monthly activity, while the minimum monthly activity values are the smallest for the whole summer season from August to December (Fig. 8). It may suggest more complex relation than pure seasonal variations. However, it is also clear that main activity increase was observed in first one and a half year after refilling of reservoir (Fig. 1), which may suggest that delayed gap influence overlapped with seasonal variations. Additionally, correlation analysis with non-overlapping time windows of various sizes didn't result in any significant short-term correlation between b-value/ EP/ MRP and water level. Such a dynamic is similar to what was observed at the beginning of the reservoir's exploitation in 2012 during the gap, when about two months after draining the water from the reservoir, the biggest earthquakes occurred (Wiszniowski et al., 2015). Despite this fact, the delayed response type of RTS in the STR2 area was considered (Gahalaut et al., 2016; Lizurek et al., 2017; Wiszniowski et al., 2015).

Here, for the first time, we were able to identify a pattern and a relation between reservoir exploitation parameters and seismic activity. Taking into account the relation between the initiation of seismicity after the first significant draining of the reservoir and the observed seasonal seismic activity changes, STR2 seismicity should be considered as a case of protracted seismic activity. The pore pressure-driven origin of seismicity with seasonal water level changes is supported by the focal mechanism solutions. The stress orientation was obtained from the available MT solutions for low and high water level periods. During high water level periods, principal stress σ_1 is rotated to WNW, while low water level periods are characterized by σ_1 and σ_2 orientations (Fig. 10), similar to the stress orientations of the whole area (Fig. 5). The difference in σ_1 orientations is within the 90% confidence areas of the inversion, which can suggest it may be an effect of the inversion uncertainty. However, a role played by the water level fluctuations and subsequent pore pressure changes in the stress orientation rotation cannot be ruled out. It is worth mentioning that the water level change is not bigger than 35 m, corresponding to a change in water load pressure of about 0.3 MPa just below the reservoir bottom if we do not take into account the bathymetry and the lithology. Much smaller stress changes (~0.01 MPa) are required to trigger earthquakes (e.g., King et al., 1994). The most well-known cases of reservoir-induced seismicity, such as Koyna and Nurek dam cases, involve impoundment depths of 100 m (1 MPa of water mass load) or more, but cases in which the impoundment depths were much smaller are also known, such as the Monticello in South Carolina, where the first earthquake occurred when the water level had been increased by 10 m, which equals to 0.1 MPa (eg. Gupta, 1992; Scholz, 2019). Moreover, post-seismic event changes of about 0.005 MPa have been shown to influence future seismicity in underground mines (e.g., Orlecka-Sikora, 2010). Furthermore, Hardebeck et al. (1998) suggest that any small stress change is capable of triggering events. Therefore, the water level-related changes observed in the STR2 reservoir may be sufficient to trigger shallow earthquakes. Our stress inversion results indicate that the area is characterized by a normal faulting regime, in contrast to the regional strike-slip trend assumed by Gahalaut et al. (2016) and further used in Coulomb stress modeling for possible faults and two strike-slip events from April 2015 by Tuan et al. (2017). Strike-slip events are sparse in this area, being observed only in the central part of the reservoir, while events in the northern part, where most of the activity took place have been characterized by normal faulting focal mechanisms with a very small strike-slip component (Lizurek et al., 2017, Fig. 4). The nodal planes azimuths of both types are similar and parallel to the Song Gia fault. Strike-slip events obtained by Tuan et al. (2017) were included in our stress inversion, but they did not significantly influence the general stress pattern dominated by normal focal mechanisms.

5. Conclusions

A statistically significant relation between water level change and increased seismic activity is found for the gap period. The gap of the reservoir filling has a substantial influence on seismicity in the STR2 vicinity. The exceedance probability of $M \geq 3.5$ events is considerably higher in the one year gap period than before the lake was drained as well as after the refilling. We also proved that the seismicity recorded between 2013 and 2016 manifested seasonal trends related to water level changes during wet and dry seasons. It is very likely, that seismic activity in the vicinity of STR2 is related to the seasonal cycle of filling the reservoir during the wet-summer season and releasing the water during the dry-winter season. The average activity was highest in February and July during the 3.5 years of post-gap period observations (Fig. 7 and Fig. 8). The rise in activity observed in the annual cycle represents a delay of two to three months to the water level change related to the seasonal filling and the draining of the reservoir's water. The average activity is higher during dry in comparison to the wet period. The response of activity and its delay with respect to water level

changes as well as the increased hazard during the gap period suggest that the main triggering factor is pore pressure change due to the significant water level changes. Seasonality related to the water level may be also involved in the principal stress orientation rotation (Fig. 10). The principal stress σ_1 orientation during the dry period is rotated about 20° toward the NW in comparison to the stress orientation derived from focal mechanisms for the wet period. It may be an artifact of inversion or feature of the seismic process. Due to overlapping of the confidence intervals it can't be ruled out it is insignificant. More focal mechanisms would be needed to solve it. Despite the strike-slip regime of the whole region, the STR2 area is characterized by a normal faulting regime, with events with a small strike-slip component being the minority. The magnitude of pore pressure changes seems to be too small for triggering events on main discontinuities, but it is enough to release the accumulated stress on smaller normal faults by change of the horizontal stresses and normal stress related to water level change and pore pressure diffusion. These findings support the previous thesis concerning reservoir exploitation-related pore pressure changes constituting the main factor triggering existing faults' seismicity (Lizurek et al., 2017; Wiszniowski et al., 2015), but not the main discontinuities, where slip is determined by the regional stress regime.

Data and resources

Data access, the computation of seasonal trends, and some image construction were carried out with the support of the EPOS Thematic Core Service Anthropogenic Hazards platform EPISODES (https://tcs.ah-epos.eu, last accessed October 25, 2021). Seismic catalog, waveforms, seismic network metadata, and water level are available on the above-mentioned platform: https://tcs.ah-epos.eu/#episode:SONG_TRANH

The software used for exponentiality test is also available in EPISODES platform (Leptokaropoulos et al., 2019; Orlecka-Sikora et al., 2020) for online application (https://tcs.ah-epos.eu) or can be downloaded from the following repository https://git.plgrid.pl/projects/EA/repos/sera-applications/browse/Magnitude_Complexity_TOOL BOX_D23_2. SHAPE software package (Seismic HAzard Parameters Evaluation) can be downloaded from https://git.plgrid.pl/projects/EA/repos/sera-applications/browse/SHAPE_Package (last accessed August 2020). MATLAB version R2017b (v.R2017b, www.mathworks.com/products/matlab, last accessed July 2020) or later is required together with the statistics and machine learning toolbox.

Stress inversion software named Stressinverse and created by Václav Vavryčuk is available via https://www.ig.cas.cz/en/stress-inverse/

Credit author statement

Grzegorz Lizurek: Conceptualization, Methodology: moment tensor. Investigation of seasonal changes. Writing- original draft, Writing - review and editing. Konstantinos Leptokaropoulos: Investigation of Probabilistic Hazard and seasonal changes of its parameters. Writing-original draft, Writing - review and editing. Jan Wiszniowski: Methodology. Software. Data curation. Writing - review and editing. Nguyen Van. Giang: Data curation: Meteorological and water level data preparation and interpretation. Izabela Nowaczyńska: Methodology of stress inversion calculation. Writing- original draft. Beata Plesiewicz: Visualisation, Dinh Quoc Van: Data curation: seismological and tectonics. Anna Tymińska: Investigation of moment tensor, Methodology of moment tensor validation. Writing - review and editing.

Declaration of Competing Interest

The authors declare that they have no known competing financial interests or personal relationships that could have appeared to influence the work reported in this paper.

Acknowledgments

References

Aki, K., Richards, P.G., 2002. Quantitative Seismology. University Science Books, Sausalito.

Bratt, S.R.T.C., Bache, C.T., 1988. Location estimation using regional array data. Bull. Seismol. Soc. Am. 78, 780–798.

Braun, T., Cesca, S., Kuhn, D., Martirosian-Janssen, A., Dahm, T., 2018. Anthropogenic seismicity in Italy and its relation to tectonics: state of the art and perspectives. Anthropocene 21, 80–94. https://doi.org/10.1016/j.ancene.2018.02.001.

Davies, R., Foulger, G., Bindley, A., Styles, P., 2013. Induced seismicity and hydraulic fracturing for the recovery of hydrocarbons. Mar. Pet. Geol. 45, 171–185.

De Natale, G., Iannaccone, G., Martini, M., Zollo, A., 1987. Seismic sources and attenuation properties at the Campi Flegrei volcanic area. Pure Appl. Geophys. 125, 883–917.

Fitch, T.J., McCowan, D.W., Shields, M.W., 1980. Estimation of seismic moment tensor from teleseismic body wave data with application to intraplate and mantle earthquakes. J. Geophys. Res. 85, 3817–3828.

Foulger, G.R., Wilson, M.P., Gluyas, J.G., Julian, B.R., Davies, J., 2018. Global review of human-induced earthquakes. Earth Sci. Rev. 178, 438–514. https://doi.org/10.1016/j.earscirev.2017.07.008.

Gahalaut, K., Tuan, A.T., Purnachandra Rao, N., 2016. Rapid and delayed earthquake triggering by the Song Tranh 2 Reservoir, Vietnam. Bull. Seismol. Soc. Am. 106, 2389–2394. https://doi.org/10.1785/0120160106.

Ge, S., Liu, M., Lu, N., Godt, J.W., Luo, G., 2009. Did the Zipingpu reservoir trigger the 2008 Wenchuan earthquake? Geophys. Res. Lett. 36, L20315 https://doi.org/10.1029/2009GL040349.

Gephart, J.W., Forsyth, W.D., 1984. An improved method for determining the regional stress tensor using earthquake focal mechanism data: application to the San Fernando earthquake sequence. J. Geophys. Res. 89, 9305–9320.

Grasso, J.-R., Karimov, A., Amorese, D., Sue, C., Voisin, C., 2018. Patterns of reservoir-triggered seismicity in a low-seismicity region of France. Bull. Seismol. Soc. Am. 108, 2967–2982. https://doi.org/10.1785/0120180172.

Gupta, H.K., 1992. Reservoir induced earthquakes. Dev. Geotech. Eng. 64.

Gupta, H.K., 2002. A review of recent studies of triggered earthquakes by artificial water reservoirs with special emphasis on earthquakes in Koyna, India. Earth Sci. Rev. 58, 279–310.

Hardebeck, J.L., Nazareth, J.J., Hauksson, E., 1998. The static stress change triggering model: constraints from two southern California aftershock sequences. J. Geophys. Res. 103 (B10), 24 427–24 437.

Hoai, L.T.T., Vuong, N.V., Dong, V.B., 2014. The characteristics of active faults and its relationship to the trigger seismicity of Song Tranh 2 dam, Bac Tra My district, Quang Nam province (center of Vietnam). VNU J. Sci. Sci. Technol. 30, 21–32.

IPONRE, 2009. Vietnam Assessment Report on Climate Change. Government of Viet Nam, Institute of Strategy and Policy on Natural Resources and Environment, Ha Noi, p. 127.

IS EPOS, . Episode: SONG TRANH. https://tcs.ah-epos.eu/#episode:SONG_TRANH. https://doi.org/10.25171/InstGeoph_PAS_ISEPOS-2017-002.

Kagan, Y.Y., 1991. 3-D rotation of double-couple earthquake sources. Geophys. J. Int. 106 (3), 709–716.

Kijko, A., Sellevoll, M.A., 1989. Estimation of earthquake hazard parameters from incomplete data files. Part I. Utilization of extreme and complete catalogs with different threshold magnitudes. Bull. Seismol. Soc. Am. 79 (3), 645–654.

King, G.C.P., Stein, R.S., Lin, J., 1994. Static stress changes and the triggering of earthquakes. Bull. Seismol. Soc. Am. 84, 935–953.

Kwiatek, G., Martínez-Garzón, P., Bohnhoff, M., 2016. HybridMT: a MATLAB/shell environment package for seismic moment tensor inversion and refinement. Seismol. Res. Lett. 87 https://doi.org/10.1785/0220150251.

Lasocki, S., Urban, P., 2011. Bias, variance and computational properties of the Kijko's estimators of the upper limit of magnitude distribution, Mmax. Acta Geophys. 59, 659–673. https://doi.org/10.2478/s11600-010-0049-y.

Lemarchand, N., Grasso, J.-R., 2007. Interactions between earthquakes and volcano activity. Geophys. Res. Lett. 34, L24303 https://doi.org/10.1029/2007GL031438.

Leptokaropoulos, K., 2020. Magnitude distribution complexity and variation at the Geysers geothermal field. Geophys. J. Int. 222, 893–906. https://doi.org/10.1093/gji/ggaa208.

Leptokaropoulos, K., Lasocki, S., 2020. SHAPE: a Matlab software package for time-dependent seismic hazard analysis. Seismol. Res. Lett. 91, 1867–1877. https://doi.org/10.1785/0220190319.

Leptokaropoulos, K., Cielesta, S., Staszek, M., Olszewska, D., Lizurek, G., Kocot, J., Lasocki, S., Orlecka-Sikora, B., Sterzel, M., Szepieniec, T., 2019. IS-EPOS: a platform for anthropogenic seismicity research. Acta Geophys. 67, 299–310. https://doi.org/10.1007/s11600-018-0209-z.

Lizurek, G., 2017. Full moment tensor inversion as a practical tool in case of discrimination of tectonic and anthropogenic seismicity in Poland. Pure Appl. Geophys. 174 (1), 197–212. https://doi.org/10.1007/s00024-016-1378-9.

Lizurek, G., Wiszniowski, J., Van Giang, N., Plesiewicz, B., Van, D.Q., 2017. Clustering and stress inversion in the Song Tranh 2 reservoir, Vietnam. Bull. Seismol. Soc. Am. 107, 2636–2648. https://doi.org/10.1785/0120170042.

Lizurek, G., Wiszniowski, J., Giang, N.V., Van, D. Q, Dung, L. V., Tung, V.D., Plesiewicz, B. (2019). Background seismicity and seismic monitoring in the Lai Chau reservoir area. J. Seismol. 23(6), pp. 1373-1390, DOI: https://doi.org/10.1007/s10950-019-09875-6, pp. 1373-1390.

McGarr, A., Simpson, D., 1997. A broad look at induced and triggered seismicity. In: Gibowicz, S.J., Lasocki, S. (Eds.), Rockbursts and Seismicity in Mines, pp. 385–396. Balkema.

Michael, A.J., 1984. Determination of stress from slip data: faults and folds. J. Geophys. Res. 89, 11 517–11 526.

Orlecka-Sikora, B., 2008. Resampling methods for evaluating the uncertainty of the nonparametric magnitude distribution estimation in the probabilistic seismic hazard analysis. Tectonophysics 456 (1–2), 38–51. https://doi.org/10.1016/j.tecto.2007.01.026.

Orlecka-Sikora, B., 2010. The role of static stress transfer in mining-induced seismic events occurrence, a case study of the Rudna mine in the Legnica-Glogow Copper District in Poland. Geophys. J. Int. 182, 1087–1095. https://doi.org/10.1111/j.1365-246X.2010.04672.x.

Orlecka-Sikora, B., Lasocki, S., Kocot, J., Szepieniec, T., Grasso, J.-R., Garcia-Aristizabal, A., Schaming, M., Urban, P., Jones, G., Stimpson, I., et al., 2020. An open data infrastructure for the study of anthropogenic hazards linked to georesource exploitation. Sci. Data 7, 89. https://doi.org/10.1038/s41597-020-0429-3.

Page, R., 1968. Aftershocks and microaftershocks of the great Alaska earthquake of 1964. Bull. Seismol. Soc. Am. 58 (3), 1131–1168.

Richter, C.F., 1936. An instrumental earthquake magnitude scale. Bull. Seismol. Soc. Am. 1–32.

Richter, C.F., 1958. The magnitude scale. In: Richter, C.F. (Ed.), Elementary Seismology, 578. Freeman, San Francisco, pp. 338–345.

Scholz, C., 2019. The Mechanics of Earthquakes and Faulting, 3rd ed. Cambridge University Press, Cambridge. https://doi.org/10.1017/9781316681473.

Simpson, D.W., Leith, W.S., Scholz, C.H., 1988. Two types of reservoir-induced seismicity. Bull. Seismol. Soc. Am. 78, 2025–2040.

Stierle, E., Bohnhoff, M., Vavryčuk, V., 2014a. Resolution of non-double-couple components in the seismic moment tensor using regional networks–II: application to aftershocks of the 1999 Mw 7.4 Izmit earthquake. Geophys. J. Int. 196, 1878–1888. https://doi.org/10.1093/gji/ggt503.

Stierle, E., Vavryčuk, V., Šílený, J., Bohnhoff, M., 2014b. Resolution of non-double-couple components in the seismic moment tensor using regional networks–I: a synthetic case study. Geophys. J. Int. 196, 1869–1877. https://doi.org/10.1093/gji/ggt502.

Tahir, M., Grasso, J.-R., Amorèse, D., 2012. The largest aftershock: how strong, how far away, how delayed? Geophys. Res. Lett. 39, L04301 https://doi.org/10.1029/2011GL050604.

Talwani, P., 1997. On the nature of reservoir-induced seismicity. Pure Appl. Geophys. 150, 473–492.

Thuy, N.N., Phach, V.V., Chinh, L.H., Minh, P.D., Nguyen, P.Q., Hung, Duong, N.A., 2003. Report on estimation of the seismic design for the Song Tranh 2 hydropower construction. In: Archives of the Institute of Geophysics. Vietnamese Academy of Science and Technology VAST, Hanoi.

Tuan, A.T., Rao, P.N., Gahalaut, K., Trong, D.C., Dung, V.L., Chien, C., Mallika, K., 2017. Evidence that earthquakes have been triggered by reservoir in the Song Tranh 2 region, Vietnam. J. Seismol. 21, 1131–1143. https://doi.org/10.1007/s10950-017-9656-2.

Valoroso, L., Improta, L., Chiaraluce, L., Di Stefano, R., Ferranti, L., Govoni, A., Chiarabba, C., 2009. Active faults and induced seismicity in the Val d'Agri area (Southern Apennines, Italy). Geophys. J. Int. 178, 488–502. https://doi.org/10.1111/j.1365-246X.2009.04166.x.

Vavryčuk, V., 2014. Iterative joint inversion for stress and fault orientations from focal mechanisms. Geophys. J. Int. 199, 69–77. https://doi.org/10.1093/gji/ggu224.

Wessel, P., Luis, J.F., Uieda, L., Scharroo, R., Wobbe, F., Smith, W.H.F., Tian, D., 2019. The generic mapping tools version 6. Geochem. Geophys. Geosyst. 20, 5556–5564. https://doi.org/10.1029/2019GC008515.

Wiejacz, P., 1992. Calculation of seismic moment tensor for mine tremors from the Legnica-Głogów Copper Basin. Acta Geophys. Pol. 40, 103–122.

Wiemer, S., Wyss, M., 2000. Minimum magnitude of completeness in earthquake catalogs: examples from Alaska, the Western United States, and Japan. Bull. Seismol. Soc. Am. 90, 859–869.

Wiszniowski, J., Giang, N.V., Plesiewicz, B., Lizurek, G., Van, D.Q., Khoi, L.Q., Lasocki, S., 2015. Preliminary results of anthropogenic seismicity monitoring in the region of Song Tranh 2 Reservoir, Central Vietnam. Acta Geophys. 63, 843–862.